Journal of Chemical Crystallography (2020) 50:400–409
https://doi.org/10.1007/s10870-019-00812-6

ORIGINAL PAPER

Synthesis, Crystal Structures, Density Functional Theory (DFT) Calculations and Molecular Orbital Calculations of Two New Metal-Free Macrocyclic Schiff Bases Derived from 2,6-Dibenzoyl-4-alkylphenol and Diamines

Javeed A. Ganaie[1] · Neha Sen[1] · Ray J. Butcher[2] · Jerry P. Jasinski[3] · Sushil K. Gupta[1]

Received: 24 May 2018 / Accepted: 31 October 2019 / Published online: 16 November 2019

Abstract

Two new phenol-based metal-free macrocyclic Schiff bases, cyclo-bis{2-[benz(N-propan-1,3-diyl)imidoyl][6-benzimidoyl][4-methyl]phenol} and cyclo-bis{2-[benz(N-butan-1,4-diyl)imidoyl][6-benzimidoyl][4-*tert*-butyl]phenol} have been synthesized and their structures determined by single crystal X-ray crystallography. The DFT geometry optimization calculations were performed to compare experimental and theoretical results. A comparison of the dihedral angles between mean planes of the central phenolato rings and peripheral phenyl rings in the crystal with the DFT theoretical calculations has been included for each molecule. Electronic transitions have been predicted by DFT molecular orbital calculations and compared with experimental absorption spectral data.

Graphic Abstract

A one-pot synthesis, crystal structure and theoretical calculations of 20- and 22-membered macrocyclic ligands are reported.

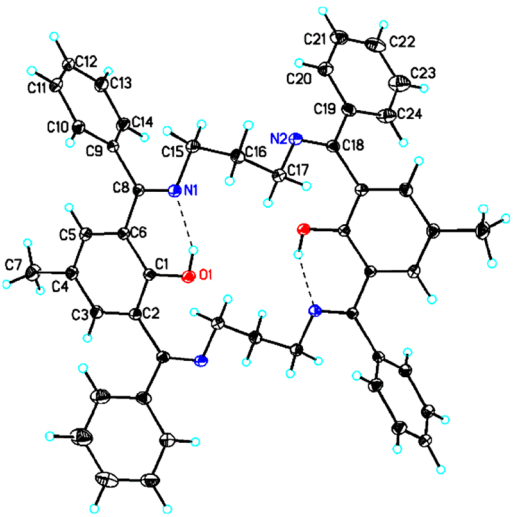

$C_{48}H_{44}N_4O_2$

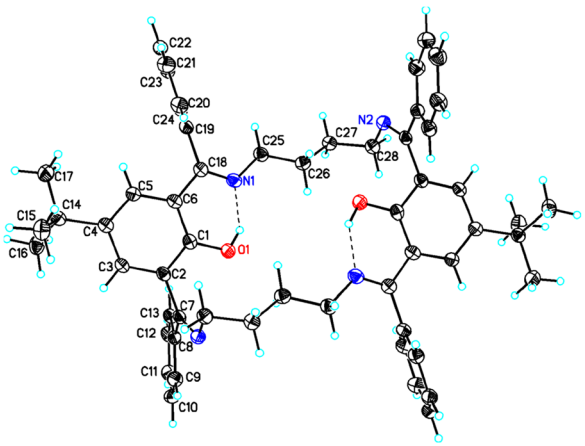

$C_{56}H_{60}N_4O_2$

Keywords Phenol-based macrocyclic derivatives · Crystal structure · DFT geometry optimization calculations · DFT molecular orbital calculations

Electronic supplementary material The online version of this article (https://doi.org/10.1007/s10870-019-00812-6) contains supplementary material, which is available to authorized users.

Extended author information available on the last page of the article

Introduction

Macrocyclic Schiff bases have potential applications as models for protein metal binding sites, synthetic ionophores, magnetic exchange phenomena, therapeutic reagents, cyclic antibiotics, host–guest interaction and in phase transfer catalysis [1, 2]. A large variety of [1 + 1] and [2 + 2] macrocyclic ligands have been synthesised by a template procedure in the presence of suitable metal ions [3]. There are various reports of metal-free macrocycles [4–6] available in the literature involving cyclodextrines [7–12], shape persistent macrocycles [13–20] and crown ethers, spherands and cryptands [21–26]. We have previously reported the synthesis and crystal structure of a neutral tetraiminodiphenol macrocycle with a C2 lateral chain, cyclo-bis{2-[benz(N-ethan-1,3-diyl)imidoyl][6-benzimidoyl] [4-methyl]phenol}, cyclo-[$L^{Me}H_2$] (n = 2) (**I**) [27]. As part of our study on phenol-based Schiff bases [28–32], we herein report the synthesis and crystal structures of cyclo-bis{2-[benz(N-propan-1,3-diyl)imidoyl][6-benzimidoyl][4-methyl]phenol}, Cyclo-[$L^{Me}H_2$] (n = 3) (**II**) and cyclo-bis{2-[benz(N-butan-1,4-diyl)imidoyl][6-benzimidoyl][4-*tert*-butyl]phenol}, Cyclo-[$L^{t\text{-}Bu}H_2$] (n = 4) (**III**), and theoretical calculations of **I**, **II** and **III** (Scheme 1) with C2, C3 and C4 lateral chains.

Experimental

Synthesis of Metal-Free Macrocyclic Ligands

The metal-free macrocyclic Schiff base ligands were synthesised by the Schiff base condensation of 4-R-2,6-dibenzoyl phenol (where R = Me, Bu^t) with propane-1,3-diamine/butane-1,4-diamine in dry THF under inert atmosphere. The synthetic scheme for (**II**) and (**III**) is given in Scheme 2. The detailed synthetic procedure and characteristics of the macrocyclic ligands are given below.

Cyclo-bis{2-[benz(N-propan-1,3-diyl)imidoyl][6-benzimidoyl][4-methyl]phenol}

Cyclo-[$L^{Me}H_2$] (II)

To a solution of 4-methyl-2,6-dibenzoylphenol (0.632 g, 2.00 mmol) in dry THF (30 mL), a solution of propane-1,3-diamine (0.158 g, 2.00 mmol) in dry THF (30 mL) was added over approximately 30 min via a dropping funnel. The solution turned yellow while it was constantly stirred for 2 h at room temperature. The resulting solution was allowed to stand for one week, during which yellow crystals of **II** formed. The crystals were filtered off, washed with cold ethanol and dried in air. Yield: 60 mg, 60%; mp 478 K.

Anal Calc for (**II**), $C_{48}H_{44}N_4O_2$ (%): C, 81.33; H, 6.26; N, 7.90. Found: C, 81.60; H, 6.15; N, 8.12. ESI–MS: *m/z*: 709 $[MH]^+$. ^{1}H NMR (300 MHz, $CDCl_3$) δ 1.73 (s, 4H, mid-CH_2); δ 2.21 (s, 6H, CH_3); δ 3.29 (m, 8H, NCH_2); δ 6.61–7.85 (m, 24H, C_6H_2 & C_6H_5); δ 16.27 (s br, 2H, OH).

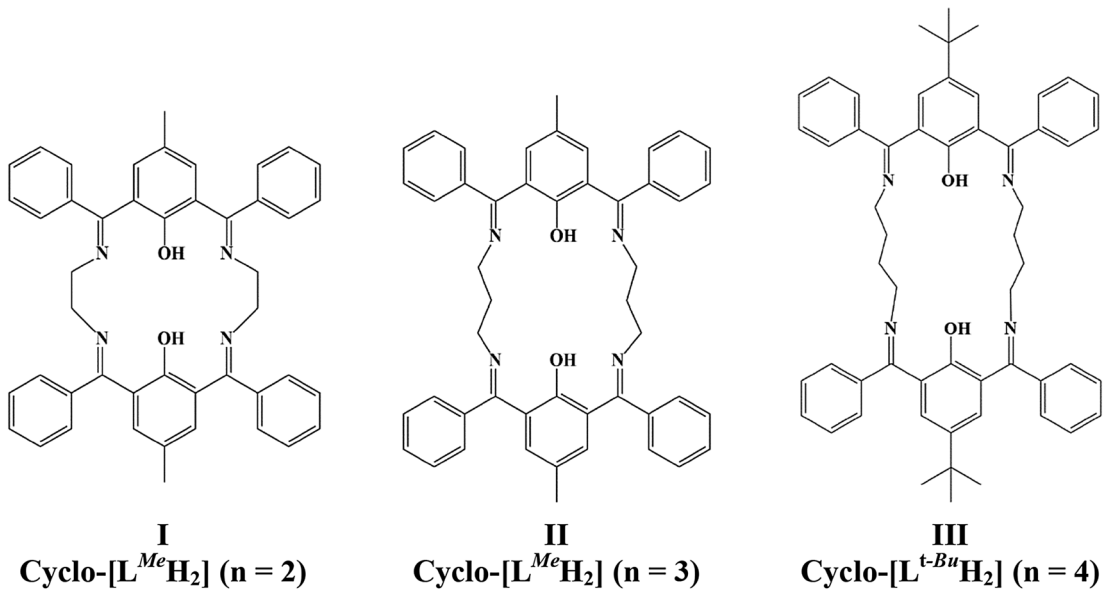

Scheme 1 Schematic diagrams of structures **I**, **II** and **III**

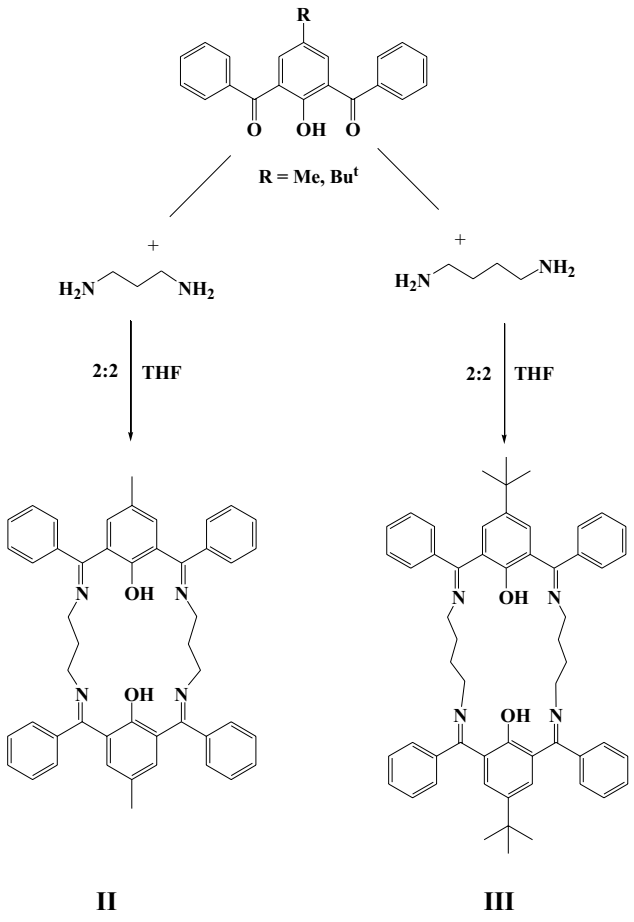

Scheme 2 Synthesis of **II** and **III**

^{13}C NMR (75 MHz, $CDCl_3$): δ 20.4 (CH_3); δ 48.9 (CH_2); 119.4, 124.1, 125.0, 127.8, 128.2, 129.4, 131.4, 133.0, 133.8, 134.2, 136.6, 137.9, 139.4 (aromatic carbon); 160.4 (C···O); 174.7 (C=N). UV–Vis (nm) (ε/L mol^{-1} cm^{-1}) (CH_3CN): 429 (217), 378 (3564), 254 (4785).

Cyclo-bis{2-[benz(N-butan-1,4-diyl)imidoyl][6-benzimidoyl][4-*tert*-butyl]phenol}

Cyclo-[L$^{t\text{-}Bu}$H$_2$] (III)

To a solution of 4-*tert*-butyl-2,6-dibenzoylphenol (0.716 g, 2.00 mmol) in dry THF (30 mL), a solution of butane-1,4-diamine (0.172 g, 2.00 mmol) in dry THF (30 mL) was added over approximately 30 min via a dropping funnel. The solution turned yellow and was stirred for 2 h at room temperature. The resulting solution was allowed to stand for 1 week, during which yellow crystals of **III** formed. The crystals were filtered off, washed with cold ethanol and dried in air. Yield: 80 mg, 65%; mp 483 K.

Anal Calc for (**III**), $C_{56}H_{60}N_4O_2$ (%): C, 81.91; H, 7.37; N, 6.82. Found: C, 82.20; H, 7.20; N, 6.60. ESI-MS: *m/z*: 820 [MH]$^+$. ^{1}H NMR (300 MHz, $CDCl_3$) δ 1.29 (s, 18H, CH_3); 1.72 (s, 8H, mid-CH_2); δ 3.56 (m, 8H, NCH_2); δ 6.81–7.65 (m, 24H, C_6H_2 & C_6H_5); δ 16.30 (s br, 2H, OH). ^{13}C NMR (75 MHz, $CDCl_3$) δ 31.2 (Me); δ 34.4 (CMe_3); δ 30.4, 48.5 (CH_2); 124.4, 128.7, 129.6, 131.0, 133.0, 133.5, 134.6, 138.2, 139.0 (aromatic carbon); 164.6 (C···O); 175.6 (C=N). UV–Vis (nm) (ε/L mol^{-1} cm^{-1}) (CH_3CN): 430 (220), 380 (3600), 258 (4800).

X-ray Structure Determination

Diffraction data were collected with a Rigaku Oxford Diffraction Gemini Ruby CCD diffractometer using graphite monochromated, Mo-Kα radiation (wavelength 0.710732 Å) for **II** and Cu-Kα radiation (wavelength 1.54178 Å) for **III** at 123 K. Absorption corrections were made by multi-scan and analytical methods using the *CrysAlisPro* software [33]. The structures were solved by direct methods using *SHELXT* [34] and all of the non-hydrogen atoms were refined anisotropically by full-matrix least-squares on F^2 using *SHELXL*2018 [35]. Hydrogen atoms were placed in their calculated positions and then refined using the riding model. The programs *SHELXTL* and XP were used for graphics [36]. X-ray data collection and structure refinements are given in Table 1.

ORTEP diagrams [37] of **II** and **III** are displayed in Figs. 1 and 2 while the crystal packing is shown in Figs. 3 and 4, respectively. Geometrically optimized structures of the molecules for **I**, **II** and **III** are shown in Fig. 5. Bond lengths and bond angles are all within expected ranges [38]. Hydrogen bonds and weak intermolecular interactions for **II** and **III** are listed in Table 2.

Computational Details

Theoretical DFT molecular orbital calculations (*WebMo Pro* [39] with the Gaussian-03 program package [40]) employing the B3LYP (Becke three parameter Lee–Yang–Parr exchange correlation functional), which combines the hybrid exchange functional of Becke [41] with the gradient correlation functional of Lee, Yang and Parr [42] and the 6-31 G(d) basis set [43] were performed for **II** and **III**. No solvent corrections were made in these calculations. Starting geometries were taken from X-ray refinement data. The optimized results in the free molecule state are, therefore, compared to those in the crystalline state. Experimentally determined oscillator strengths (*f*) were determined by use of an equation relating them to the molar decadic absorption coefficient (ε) ($f = 4.32 \times 10^{-9} \cdot \varepsilon_{max} \cdot \Delta\omega_{1/2}$) [44–46]. The molar decadic absorption coefficient measures the intensity of the optical absorption at a given wavelength. Deconvolution of the spectra to obtain the ε_{max} and $\Delta\omega_{1/2}$ values was carried out by the Origin program [47]. Discrepancies between the experimental and calculated band centres and

Table 1 Crystal and experimental data for **II** and **III**

	II	**III**
Empirical formula	$C_{48}H_{44}N_4O_2$	$C_{56}H_{60}N_4O_2$
Formula weight	708.87	821.08
Temperature	123(2) K	123(2) K
Wavelength	0.71073 Å	1.54184 Å
Crystal system	Trigonal	Triclinic
Space group	*R*−3	*P*−1
Unit cell dimensions	*a* = 31.1743(10) Å	*a* = 6.0388(7) Å *b* = 11.4476(14) Å
	c = 10.8332(4) Å	*c* = 16.4399(12) Å α = 86.637(8)° β = 84.344(8)° γ = 88.494(10)°
Volume	9117.6(5) Å^3	1128.8(2) Å^3
Z	9	1
Density (calculated)	1.162 Mg/m^3	1.208 Mg/m^3
Absorption coefficient	0.071 mm^{-1}	0.565 mm^{-1}
F(000)	3384	440
Crystal size	0.33 × 0.28 × 0.12 mm^3	0.4561 × 0.0477 × 0.0459 mm^3
Theta range for data collection	3.31° to 34.98°	2.71° to 75.50°
Index ranges	−46 ≤ h ≤ 46, −49 ≤ k ≤ 28, −17 ≤ l ≤ 9	−7 ≤ h ≤ 5, −14 ≤ k ≤ 11, −20 ≤ l ≤ 20
Reflections collected	24,760	7440
Independent reflections	8326 [R_{int} = 0.0447]	4492 [R_{int} = 0.0620]
Completeness to theta = 25.50°	99.6%	99.4%
Absorption correction	Semi-empirical from equivalents	Analytical
Max. and min. transmission	1.00000 and 0.99515	0.976 and 0.880
Refinement method	Full-matrix least-squares on F^2	Full-matrix least-squares on F^2
Data/restraints/parameters	8326/0/246	4492/0/287
Goodness-of-fit on F^2	1.016	1.020
Final R indices [I > 2σ(I)]	R1 = 0.0764, wR2 = 0.1767	R1 = 0.0764, wR2 = 0.1998
R indices (all data)	R1 = 0.1292, wR2 = 0.2057	R1 = 0.1168, wR2 = 0.2366
Largest diff. peak and hole	0.610 and −0.313 e Å^{-3}	0.356 and −0.274 e Å^{-3}

band intensities exist. All calculations were using default convergence criteria.

Density Functional Theory (DFT) Calculations

Bond angles and bond distances observed in the crystal structure match well those obtained by the geometry optimized DFT calculations at the B3LYP 6-31G(d) level. That is, the differences between the two values are within normal ranges and are generally consistent with bond lengths and angles for similar types of compounds. In addition, a comparison of the angles between the mean planes of the *central phenolato* and *peripheral phenyl* rings in the crystal and with the DFT geometry optimized calculation have been included in a discussion of the structural aspects for each molecule. From a DFT molecular orbital calculation for each compound, surface plots for the two highest occupied molecular orbitals (HOMO, HOMO−1) and three lowest unoccupied molecular orbitals (LUMO, LUMO+1, LUMO+2) are displayed to provide a visual evidence of the molecular orbitals involved in the spectroscopic electronic energy transitions examined. Based on correlation of the energies of these HOMO–LUMO frontier surfaces to the UV–Vis absorption spectra, electronic excitation transition predications are suggested.

Results and Discussion

Structural Study of (II) and (III)

In (**II**) and (**III**), the 20-membered and 22-membered macrocyclic ligands, respectively are located on a crystallographic inversion centre with half of the molecule in the asymmetric unit (Figs. 1, 2). The phenolic hydrogen forms a hydrogen bond with donor–acceptor distances of 2.53 Å and 2.50 Å

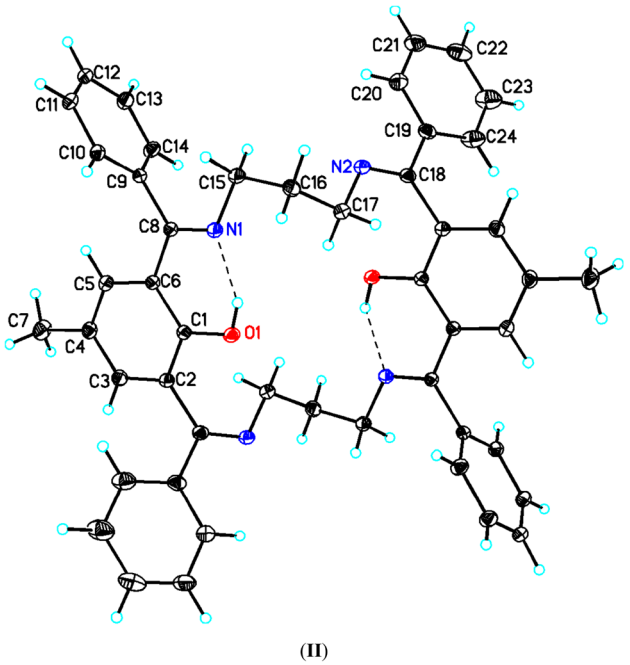

Fig. 1 ORTEP diagram for **II**, $C_{48}H_{44}N_4O_2$, showing the atom numbering scheme with 30% probability ellipsoids. Dashed lines indicate O–H···N hydrogen bonds generating *S*(6) ring motifs

to the imine nitrogen (Table 2) in **II** and **III**, respectively. The aliphatic methylene diimine groups in **II** are in a *gauche* conformation as shown by the N–C–C–C/C–C–C–N torsion angles of ca. 66°. The mean plane of the central phenolato ring (C1–C6) makes dihedral angles of 82.58(5)° and 72.88(5)° **II** and 82.05(15)° and 73.97(15)° **III**, respectively, with the peripheral phenyl rings (C9–C14) and (C19–C24) **II** and (C8–C13) and (C19–C24) **III**. Both the peripheral phenyl rings are inclined by an angle of 24.55(5)° and 18.02 (16)° in **II** and **III**, respectively. The mean phenolic C–O distance is slightly longer in **II** [1.3435(17) Å] than in **III** [1.335(4) Å].

In **II**, the molecular conformation is stabilised by classical intramolecular O–H···N hydrogen bonds generating an *S*(6) ring motif (Fig. 3). In addition, weak intermolecular C–H···O interactions involving the methylene chain and a phenolato oxygen atom (Table 2) [48] are found to influence the crystal packing.

In **III**, the macrocyclic ligand possesses both OH and NH tautomeric character in its molecular structure and is stabilized by both O–H···N and N–H···O classical intramolecular hydrogen bonds (Fig. 4, Table 2). The molecules are further linked by weak C–H···O and C–H···π interactions forming a three-dimensional network.

The observation of tautomeric character in (**III**) (Scheme 3) may be predicted due to the presence of *tert*-butyl groups that are more electron releasing than the methyl groups in (**I**) and (**II**).

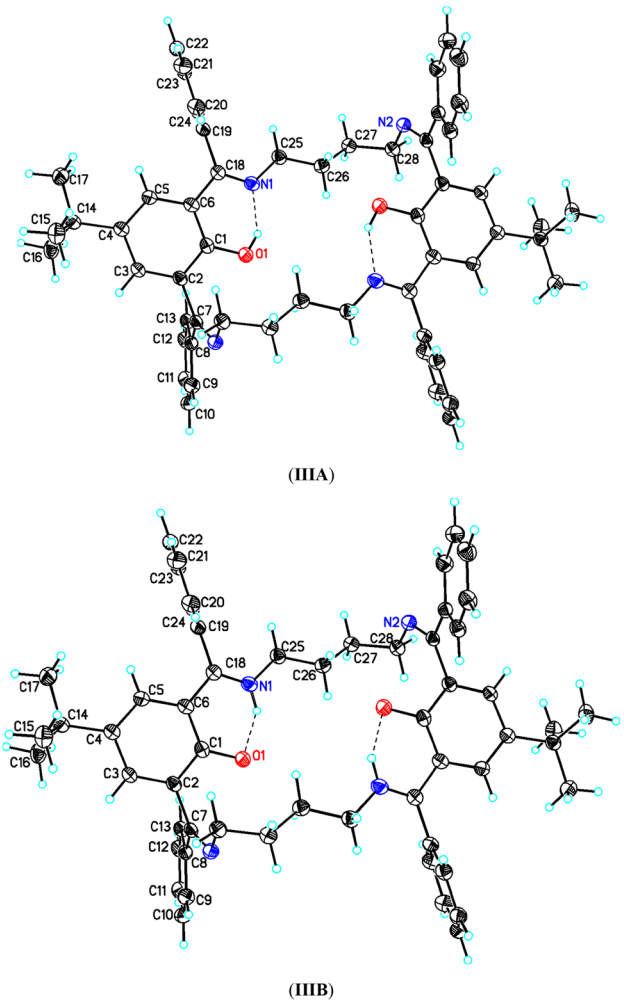

Fig. 2 ORTEP diagram for **III,** $C_{56}H_{60}N_4O_2$, showing the atom numbering scheme with 30% probability ellipsoids. Dashed lines indicate both O–H···N (**IIIA**) and N–H···O (**IIIB**) intramolecular hydrogen bonds showing tautomers

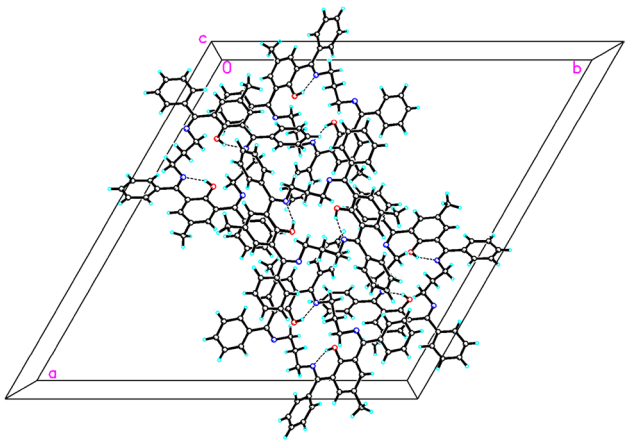

Fig. 3 Packing diagram for **II**, $C_{48}H_{44}N_4O_2$ viewed along the *c* axis showing intramolecular O–H···N hydrogen bonds

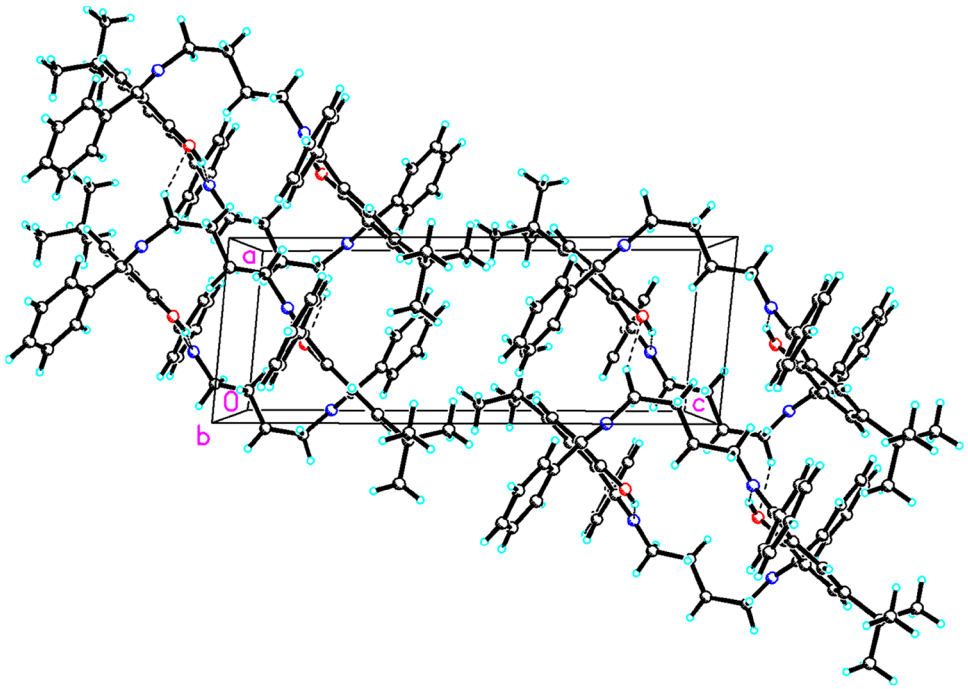

Fig. 4 Packing diagram for **III**, $C_{56}H_{60}N_4O_2$, viewed along the *b* axis showing both O–H···N and N–H···O intramolecular hydrogen bonds

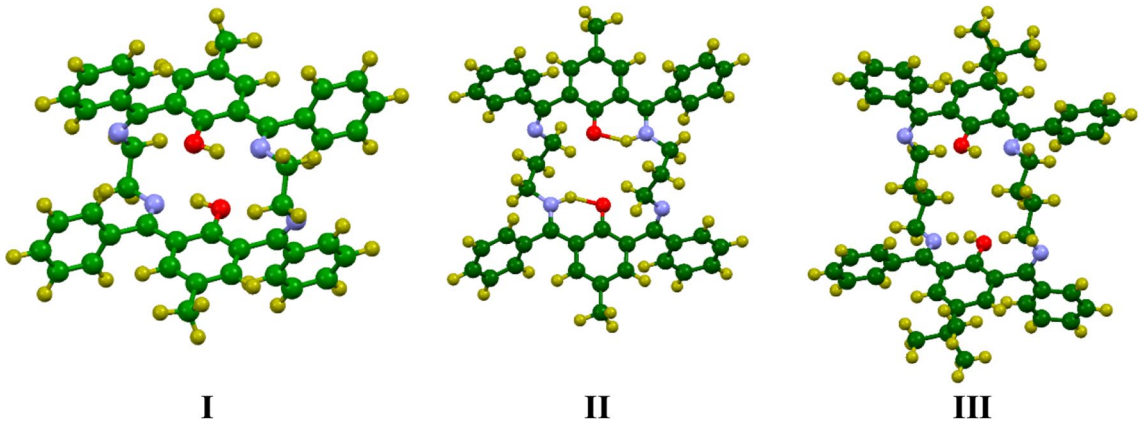

Fig. 5 **DFT** Optimized Geometries for **I**, **II** and **III**

Theoretical Study of I, II and III

The synthesis and structure of **I** was previously reported [27]. However, DFT calculations were performed to enable comparisons between **I**, **II** and **III**.

DFT Optimized Geometries

DFT geometry optimization calculations for **I**, **II** and **III** (Fig. 5) resulted in bond lengths and bond angles similar to those observed from experimental data and any small differences were unremarkable. The largest discrepancies in the bond length of **III** were in the range of 0.049 to 0.064 Å while the largest differences between the experimental and theoretical values for bond angles were between 4.50° and 6.75°. The dihedral angle between the mean planes of the central phenolato ring and peripheral phenyl rings are calculated to be 86.0(7)° and 76.4(4)° in **I** and 66.3(1)° and 67.1(9)° in **II**, slightly more twisted from those observed in the crystal structure with 82.99(8)° and 88.20(8)° for **I** and 82.58(5)° and 72.88(5)° for **II**. The calculated dihedral angle between the mean planes of the peripheral phenyl rings are 17.5(1)° **I** and 11.8(6)° **II**, compared the experimentally obtained values of 17.36(8)° and 24.55(5)°, respectively. In **III**, the dihedral angles between the mean planes of the central phenolato ring (C1–C6) and peripheral phenyl rings (C8–C13 and C19–C24) calculated to be 81.1(1)° and 73.4(3)°, are almost same as those observed in the crystal

Table 2 Hydrogen bond and intermolecular interactions for **II** and **III** [Å and °]

Cg1 is the centroid of the C9–C14 benzene ring for **III**				
D–H···A	d(D–H)	d(H···A)	d(D···A)	< (DHA)
II, $C_{48}H_{44}N_4O_2$				
O(1)–H(1)···N(1)	0.84	1.78	2.5291(16)	147.7
C(17)–H(17B)···O(1)#1	0.99	2.53	3.202(2)	124.7
III, $C_{56}H_{60}N_4O_2$				
O(1)–H(1O^a)···N(1)	0.84	1.77	2.508(4)	146.0
N(1)–H(1 N^b)···O(1)	0.88	1.75	2.508(4)	142.5
C(28)–H(28B)···O(1)#2	0.99	2.42	3.105(4)	126.2
C(16)—H(16C)···Cg1#3	0.98	2.78	3.740(6)	168.0

Symmetry codes: #1: −x+4/3, −y+5/3, −z+2/3; #2−x, −y+1, −z+2; #3: −x, −y+1, −z+2

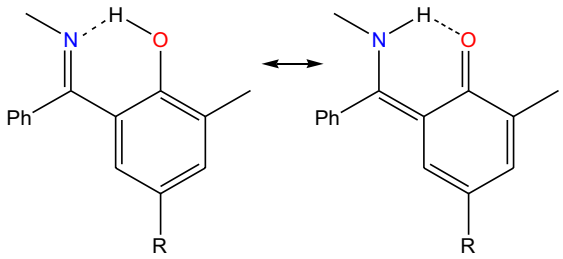

R = *tert*-butyl

Scheme 3 Tautomeric form of (**III**)

structure at 82.05(15)° and 73.97(15)°, respectively. The computed dihedral angle between the mean planes of the two peripheral phenyl rings is 26.1(1)°, an increase of 8.08(1)° compared to the experimental result. These changes support the suggestion that weak C–H···O intermolecular interactions involving the methylene chain and phenolato oxygen atom in concert with intramolecular O–H···N and N–H···O hydrogen bonds and weak C–H···π interactions involving the *tert*-butyl group and benzimidoyl ring all play a role in the crystal packing of the molecule (Table 2).

Electronic Absorption Spectra and DFT Molecular Orbital Calculations

Calculated molecular orbital energies (eV) for the surfaces of the frontier molecular orbitals for **I**, **II** and **III** are shown in Fig. 6 and Table 3.

In the HOMO−1 and HOMO for **I**, **II** and **III**, the electronic clouds are distributed primarily on both central phenolato rings. In the LUMO and LUMO+1 the electronic clouds are delocalized primarily on the central phenolato ring and imino group of the benzimidoyl ring for **I** and **II** and on the imido nitrogen on both sides in **III**. In the LUMO+2 they are dispersed primarily on the imido nitrogen and benzimidoyl rings of the opposite side in **I** and **II** while in **III** they are located only the benzimidoyl ring of one side of the ring.

The observed experimental absorption spectra show three band envelopes with λ_{max} values located at 419, 368 and 250 nm **I**, 429, 378 and 254 nm **II** and 430, 380 and 258 nm **III**, respectively. Electronic transitions are generally paired between the various molecular orbitals of the ground and excited states corresponding to these three band envelopes as indicated in Table 3. Therefore, the first absorption band envelope at 419–430 nm is assigned to contributions primarily from HOMO → LUMO and HOMO−1 → LUMO. The second absorption band at 368–380 nm is assigned to overlapping contributions from HOMO → LUMO+1 and HOMO−1 → LUMO+1. The third absorption band at 250–258 nm is assigned to overlapping contributions from HOMO → LUMO+2 and HOMO−1 → LUMO+2.

It is evident further that electron transitions among frontier molecular orbitals are corresponding to the transitions of phenolate oxygen to phenyl ring ($PhO^- \rightarrow Ph$), $n \rightarrow \pi^*$ (C=N) and $\pi \rightarrow \pi^*$ (phenyl ring) transitions.

In the present investigation, the HOMO–LUMO gap: 4.67 eV (**I**) > 4.54 eV (**II**) > 3.76 eV (**III**) is well correlated with an increasing methylene chain in (**I**), (**II**) and (**III**).

Summary and Conclusions

The crystal and molecular structure of two metal-free tetraiminodiphenol macrocyclic ligands containing C3 and C4 lateral chains, were determined. The frontier molecular orbitals of tetraiminodiphenols with the C2, C3 and C4 lateral chain were studied with density functional theory (DFT-B3LYP 6-31 G(d)) geometry optimization and molecular orbital calculations. Correlation between the calculated molecular orbital energies (eV) for the surfaces of the frontier molecular orbitals to the electronic excitation transitions from the absorption spectrum of each compound were determined. In each compound, the DFT molecular orbital calculation, supported by a geometry optimization calculation confirmed that the excitation energies of the surfaces of the frontier molecular orbitals from the HOMO−1 and HOMO to LUMO, LUMO+1 and LUMO+2 electronic excitations closely match the λ_{max} values of the absorption spectra in overlapping contributions from three excitations within each band envelope. Further, the decreasing HOMO–LUMO energy gap correlates very well with the number of methylene spacers in the diamine fragment of the Schiff base. Because of the presence of *tert*-butyl groups in **III** which are more electron releasing then the methyl groups in **I** and **II**, the former appears to be tautomer. In the crystal structures of two compounds, it has been determined that hydrogen bonds and/or weak C—H···O and C—H···π intermolecular interactions play a role in the crystal packing of

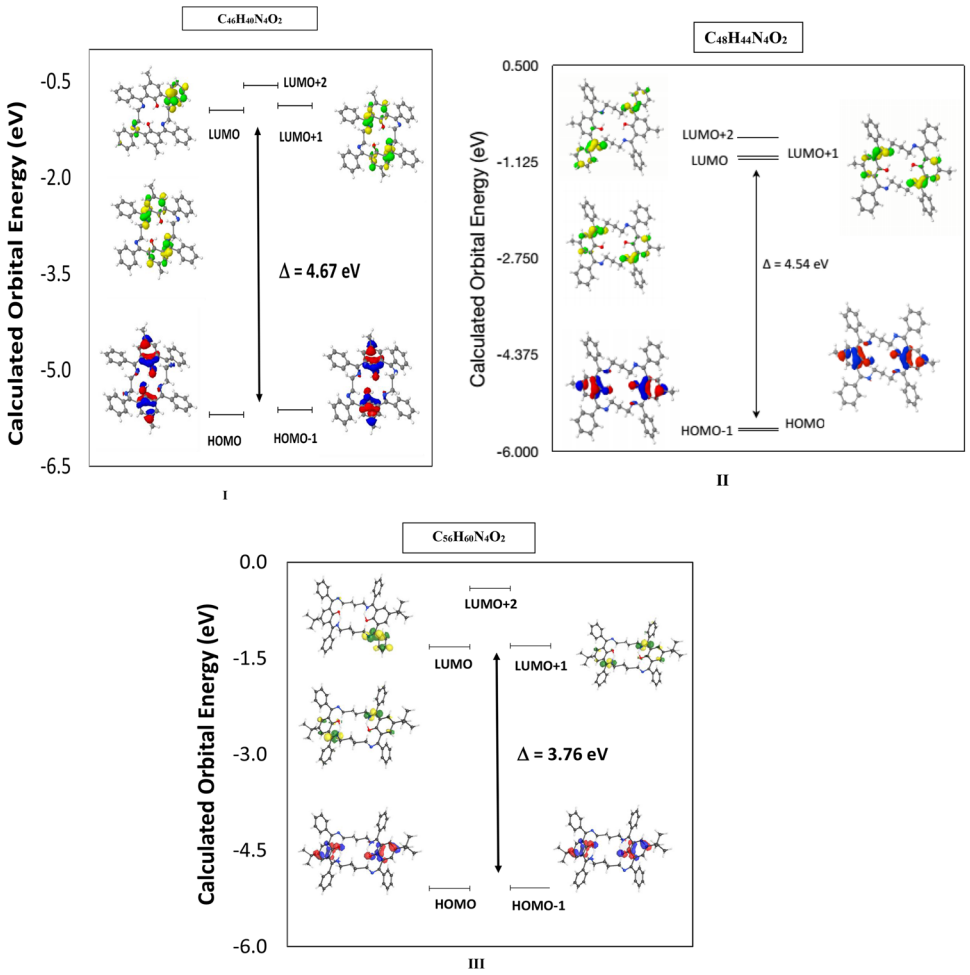

Fig. 6 Calculated frontier molecular orbitals for **I**, **II** and **III**

each molecule. This is consistent changes in the mean planes between the rings within the asymmetric unit comparing the crystal structures and to the molecular structures obtained from density functional theory (DFT) geometry optimization calculations.

Supporting Information

X-ray crystallographic files, in CIF format, for the structure determination of (**II**) (1844201) and (**III**) (1844202) have been deposited with the Cambridge Crystallographic Data Centre, CCDC:26091. Copies of this information may be obtained free of charge from the Director, CCDC, 12 Union Road, Cambridge, CB2 1EZ (fax: +44-1223-336033; email: deposit@ccdc.cam.uk or at http://www.ccdc.cam.ac.uk).

Acknowledgements Financial support from the Government of India through the Department of Science and Technology [Project no. SR/S1/IC-38/2007] and the University Grants Commission [Project no. F.37-500/2009 (SR)] is gratefully acknowledged. RJB wishes to acknowledge the National Science Foundation for funds to purchase the diffractometer.

References

1. Alexander V (1995) Chem Rev 95:273–342
2. Chu Z, Huang W, Wang L, Gou S (2008) Polyhedron 27:1079–1092
3. Tamburini S, Vigato PA (2004) Coord Chem Rev 248:1717–2128
4. Tian Y, Tong J, Frenzen G (1999) Sun J-Yu. J Org Chem 64:1442–1446
5. Atkins AJ, Black D, Blake AJ, Becerra AM, Parsons S, Ramirez LK, Schroder M (1996) Chem Commun 4:457–464
6. Tian YQ, Tong J (1997) Chin Chem Lett 8:107–110
7. Biwer A, Antranikian G, Heinzle E (2002) Appl Microbiol Biotechnol 59:609–617
8. Del Valle EMM (2010) Process Biochem 31:1033–1046
9. Thatiparti TR, Shoffstall AJ, Von Recum HA (2010) Biomaterials 31:2335–2347
10. Marcolino VA, Zanin GM, Durrant LR, Benassi MDT, Matioli GJ (2011) Agric Food Chem 59:3348–3357
11. De Oliveira V E, Almeida EWC, Castro HV, Edwards HGM, Dos Santos HF, de Oliveira LFC (2011) J Phys Chem A 115:8511–8519
12. Brusseau ML, Wang X (1997) Wang W -Z. Environ Sci Technol 31:1087–1092
13. Hoger S (2004) Chem Eur J 10:1320–1329
14. Zhang W, Moore JS (2005) J Am Chem Soc 127:11863–11870
15. Zang L, Che Y, Moore JS (2008) Acc Chem Res 41:1596–1608

Table 3 Experimental and calculated energy of molecular orbitals for **I**, **II** and **III** and their associated transitions

λ_{max} (nm/eV)	Experimental MO contributions	f	λ_{max} (nm/eV)	Calculated MO contributions
(**I**)				
419/2.95	HOMO → LUMO	0.011	265/4.67	HOMO → LUMO
419/2.95	HOMO−1 → LUMO	0.011	261/4.74	HOMO−1 → LUMO
368/3.36	HOMO → LUMO+1	0.048	261/4.74	HOMO → LUMO+1
368/3.36	HOMO−1 → LUMO+1	0.048	257/4.81	HOMO−1 → LUMO+1
250/4.95	HOMO → LUMO+2	0.055	245/5.05	HOMO → LUMO+2
250/4.95	HOMO−1 → LUMO+2	0.055	241/5.13	HOMO−1 → LUMO+2
(**II**)				
429/2.89	HOMO → LUMO	0.016	273/4.55	HOMO → LUMO
429/2.89	HOMO−1 → LUMO	0.016	270/4.59	HOMO−1 → LUMO
378/3.28	HOMO → LUMO+1	0.041	270/4.60	HOMO → LUMO+1
378/3.28	HOMO−1 → LUMO+1	0.041	267/4.64	HOMO−1 → LUMO+1
254/4.88	HOMO → LUMO+2	0.065	253/4.91	HOMO → LUMO+2
254/4.88	HOMO−1 → LUMO+2	0.065	250/4.95	HOMO−1 → LUMO+2
(**III**)				
430/2.88	HOMO → LUMO	0.028	329/3.76	HOMO → LUMO
430/2.88	HOMO−1 → LUMO	0.028	329/3.76	HOMO−1 → LUMO
380/3.26	HOMO → LUMO+1	0.054	328/3.78	HOMO → LUMO+1
380/3.26	HOMO−1 → LUMO+1	0.054	327/3.78	HOMO−1 → LUMO+1
258/4.80	HOMO → LUMO+2	0.061	265/4.67	HOMO → LUMO+2
258/4.80	HOMO−1 → LUMO+2	0.061	265/4.67	HOMO−1 → LUMO+2

Oscillator strength, $f = 4.32 \times 10^{-9} \cdot \varepsilon_{max} \cdot \Delta\omega_{1/2}$

16. Akine S, Taniguchi T, Nabeshima T (2001) Tetrahedron Lett 42:8861–8864
17. Gallant AJ, MacLachlan MJ (2003) Angew Chem Int Ed 42:5307–5310
18. Hui JK-H, MacLachlan MJ (2006) Chem Commun 23:2480–2482
19. Guieu S, Crane AK, MacLachlan MJ (2011) Chem Commun 47:1169–1171
20. Chen Z, Guieu S, White NG, Lelj F, MacLachlan MJ (2016) Chem Eur J 22:17657–17672
21. Pedersen CJ (1988) Angew Chem Int Ed Engl 27:1021–1027
22. Pedersen CJ (1967) J Am Chem Soc 86:7017–7036
23. Dietrich B, Lehn JM, Sauvage JP (1969) Tetrahedron Lett 10:2885–2888
24. Lehn J (1988) Angew Chem Int Ed Engl 27:89–112
25. Cram DJ, Kaneda T, Helgeson RC, Lein GM (1979) J Am Chem Soc 101:6752–6754
26. Cram DJ (1986) Angew Chem Int Ed Engl 25:1039–1134
27. Asatkar AK, Verma VK, Jain TA, Singh R, Gupta SK, Butcher RJ (2011) Acta Crystallogr E67:o2724–o2725
28. Gupta SK, Anjana C, Butcher RJ, Sen N (2010) Acta Crystallogr E66:m1531–m1532
29. Gupta SK, Anjana C, Sen N, Jasinski JP, Golen JA (2012) J Chem Crystallogr 42:960–967
30. Ganaie JA, Kumar J, Butcher RJ, Jasinski JP, Gupta SK (2016) J Chem Crystallogr 46:93–104
31. Gupta SK, Anjana C, Sen N, Butcher RJ, Jasinski JP, Golen JA (2015) Polyhedron 89:219–231
32. Gupta SK, Sen N, Ganaie JA, Butcher RJ, Jasinski JP (2017) J Coord Chem 70:3147–3170
33. Rigaku Oxford Diffraction (2015) *CrysAlis Pro*. The Woodlands
34. Sheldrick GM (2015) Acta Crystallogr A 71:3–8
35. Sheldrick GM (2015) Acta Crystallogr C 71:3–8
36. Sheldrick GM (2008) Acta Crystallogr A 64:112–118
37. Johnson CK (1976) *ORTEP II. Report ORNL-5138*. Oak Ridge National Laboratory, Oak Ridge
38. Allen FH, Kennard O, Watson DG, Brammer L, Orpen A, Taylor RJ (1987) Chem Soc Perkin Trans 2:S1–S19
39. Schmidt JR, Polik WF (2007) WebMO Pro, version 8.0.01e; WebMO, LLc: Holland. http://www.webmo.net
40. Frisch MJ, Trucks GW, Schlegel HB, Scuseria GE, Robb MA, Cheeseman JR, Scalmani G, Barone V, Mennucci B, Petersson GA, Nakatsuji H, Caricato M, Li X, Hratchian HP, Izmaylov AF, Bloino J, Zheng G, Sonnenberg JL, Hada M, Ehara M, Toyota K, Fukuda R, Hasegawa J, Ishida M, Nakajima T, Honda Y, Kitao O, Nakai H, Vreven T, Montgomery JA Jr, Peralta JE, Ogliaro F, Bearpark M, Heyd JJ, Brothers E, Kudin KN, Staroverov VN, Kobayashi R, Normand J, Raghavachari K, Rendell A, Burant JC, Iyengar SS, Tomasi J, Cossi M, Rega N, Millam JM, Klene M, Knox JE, Cross JB, Bakken V, Adamo C, Jaramillo J, Gomperts R, Stratmann RE, Yazyev O, Austin AJ, Cammi R, Pomelli C, Ochterski JW, Martin RL, Morokuma K, Zakrzewski VG, Voth GA, Salvador P, Dannenberg JJ, Dapprich S, Daniels AD, Farkas O, Foresman JB, Ortiz JV, Cioslowski J, Fox DJ (2009) Gaussian 09, Revision D.01. Gaussian Inc., Wallingford
41. Becke AD (1998) Phys Rev A 38:3098
42. Lee C, Yang W, Parr RG (1988) Phys Rev B 37:785
43. Hehre WJ, Random L, Schleyer PR, Pople JA (1986) Ab initio molecular orbital theory. Wiley, New York
44. Pearl GM, Zerner MC, Broo A, McKelvey J (1998) J Comput Chem 19:781–796
45. Holland JP, Barnard PJ, Bayly SR, Dilworth JR, Green JC (2009) Inorg Chim Acta 362:402–406
46. Guillaumont D, Nakamura S (2000) Dyes Pigm 46:85–92

47. Origin 8.0. Origin Lab (2007) Origin Lab Corporation, Northampton
48. Bernstein J, Davis RE, Shimoni L, Chang NL (1995) Angew Chem Int Ed Engl 34:1555–1573

Affiliations

Javeed A. Ganaie[1] · Neha Sen[1] · Ray J. Butcher[2] · Jerry P. Jasinski[3] · Sushil K. Gupta[1]

✉ Sushil K. Gupta
skggwr@gmail.com; skgupta@jiwaji.edu

[1] School of Studies in Chemistry, Jiwaji University, Gwalior 474011, India

[2] Department of Chemistry, Howard University, 525 College Street NW, Washington, DC 20059, USA

[3] Department of Chemistry, Keene State College, 229 Main Street, Keene, NH 03435-2001, USA